3-2004

High-rate growth-mode transitions in Al-Si eutectics

Ralph E. Napolitano
Iowa State University, ren1@iastate.edu

L. G. England
Iowa State University

High-rate growth-mode transitions in Al-Si eutectics

Abstract
Irregular eutectic growth in an aluminum-silicon alloy is investigated using directional solidification. The high-rate transition from flake to fiber morphology is characterized in term of the three dimensional microstructure. The transition is observed to occur over the velocity range from 100 to 1000 mm/s, and two regimes of behavior are observed using a characteristic length scale defined by the spatial variation in local volume fraction.

Keywords
Eutectic solidification, aluminium-silicon, growth transitions

Disciplines
Metallurgy

Comments
This conference proceeding is from *Solidification of Aluminum Alloys* (2004): 121. Posted with permission.

Solidification of Aluminum Alloys
Edited by Men G. Chu, Douglas A. Granger and Qingyou Han
TMS (The Minerals, Metals & Materials Society), 2004

HIGH-RATE GROWTH-MODE TRANSITIONS IN AL-SI EUTECTICS

R. E. Napolitano and L. G. England

Department of Materials Science and Engineering
2220 Hoover Hall, Iowa State University, Ames, Iowa 50011

Keywords: Eutectic solidification, aluminum-silicon, growth transitions

Abstract

Irregular eutectic growth in an aluminum-silicon alloy is investigated using directional solidification. The high-rate transition from flake to fiber morphology is characterized in terms of the three dimensional microstructure. The transition is observed to occur over the velocity range from 100 to 1000 mm/s, and two regimes of behavior are observed using a characteristic length scale defined by the spatial variation in local volume fraction.

Introduction

The alloys that are based on the Al-Si eutectic system are among the most versatile for net shape castings, offering an extensive range of properties suitable for a broad scope of engineering applications. The variety of eutectic morphologies that may develop in these alloys is equally diverse, as shown in Fig.1. The most common of these structures, shown in Fig.1(a,b) is characterized by broad faceted silicon plates or *flakes*, where strong kinetic anisotropy constrains the silicon growth to the most favorable crystallographic directions, giving rise to a nonuniform or *irregular* eutectic microstructure. This morphology is generally observed in conventional shape castings, where cooling rates are relatively low. Substantial improvements in mechanical properties are commonly achieved, however, through an intentional refinement or *modification* of the eutectic structure.

In a phenomenon known as impurity-modification, trace amounts of elements such as Sr, Na, or Ce [1,2,3] significantly alter the mechanisms of atomic attachment at the liquid-silicon interface. By initiating twin-plane reentrant edges, these impurities provide an alternative to the ledge-step propagation mechanism typical in faceted growth. Moreover, the multiplicity of twin plane possibilities facilitates the morphological self-optimization of the interface so that, at this mesoscopic scale, the impurity modified alloy solidifies much like a *regular* eutectic. In the absence of trace impurity additions, a flake to fiber transition is observed with increasing growth rates, typically between approximately 400 and 800 μm/s [4,5], as shown in Fig.1(d-h). Although this *quench-modification* involves no alloying addition, it is nevertheless related to the kinetics of the silicon-liquid interface, within the context of the overall kinetics of the irregular eutectic structure. Unlike its impurity-related counterpart, quench-modification is a gradual transition that occurs over a large range of growth rates. Accordingly, various degrees of modification may be observed. Despite the dramatic structural changes associated with quench modification, the fundamental mechanisms of adjustment and selection that give rise to this behavior have not yet been identified. Furthermore, the qualitative nature and velocity range of the quench-modification transition have not been clearly established. Observations have shown that the high-velocity fibrous structure contains nonfaceted silicon with a very low

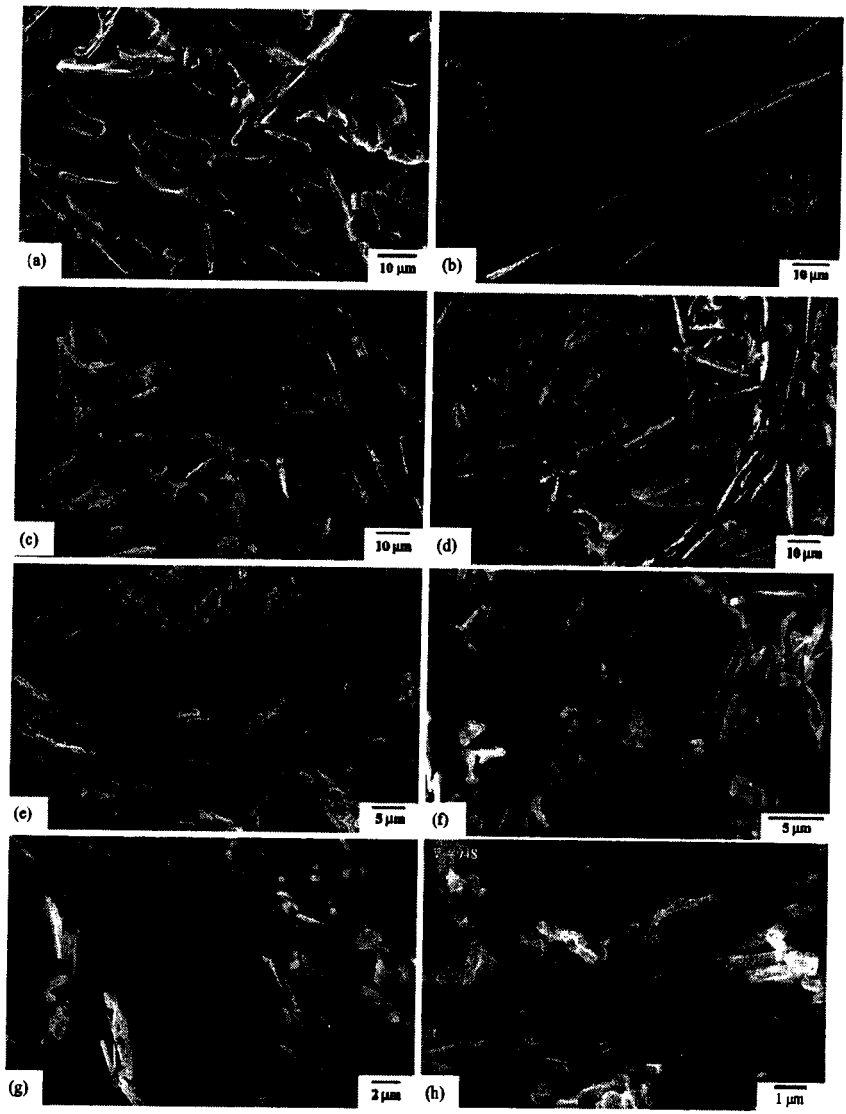

Figure 1. Typical silicon morphology after directional solidification of an Al-Si eutectic in a temperature gradient of 7.5 K/mm. Growth rates are (a) 10, (b) 20, (c) 50, (d) 95, (e) 250, (f) 500, (g) 700, and (h) 950 µm/s. The Al-rich phase has been chemically removed.

twin density [6,7]. Reports of the velocity range over which the transition occurs are limited, generally indicating that the fibrous morphology develops as velocity is increased above approximately 400 μm/s [4,5,8,9]. Several reports of the transition range are listed in Table I, and it must be noted that the observed transition range depends on the temperature gradient. The relationship between interface temperature and the quench modification transition also remains unclear. Khan and Elliott reported a dramatic decrease in interface undercooling associated with the transition [10], but Jenkinson and Hogan suggested an undercooling criterion for the transition, stating that modification occurs at undercoolings greater than 6K [11].

Table I. Reported transition velocities.

	Gradient (K/mm)	Velocity (μm/s)
Steen and Hellawell [5]	11	400-800
	23	160-200
Toloui and Hellawell [10]	8	800
Atasoy [6]	12	395-570
Cuprys [9]	4, 10, 25	400-700
Current Study	7.5	50-1000

It is generally understood that the high-velocity modification observed in Al-Si eutectics involves a transition in the silicon growth mechanism from the step-propagation of a faceted phase to the continuous growth of a nonfaceted phase [10]. However, the competition and selection mechanisms that govern this transition are not well understood, largely due to the current limitations in our understanding of selection mechanisms in the normal (flake) irregular eutectic structures. Indeed, all analytical models for eutectic growth, derived from the Jackson-Hunt (JH) approach [12,13,14,15,16], describe the interface temperature in terms of overall velocity, eutectic spacing, and phase compositions. However, the eutectic spacing, which is the sole microstructural parameter in any such treatment, is inherently insufficient to capture the physical processes involved in selection of eutectic operating state in all but the simplest of cases (i.e. regular lamellar and rod morphologies). The essence of the irregular growth problem, and any other diffusive free-boundary problem for that matter, is the partitioning of the driving free energy into the various dissipative processes such as solute diffusion, atomic attachment at the interface, and the maintenance of the interface shape. For a regular eutectic structure, each of these may conveniently be quantified in terms of a single spacing parameter, due to the strict periodicity. For an irregular eutectic, however, the simple spacing parameter is not sufficient to describe these contributions to undercooling. Despite such difficulties, reasonable success has been observed in predicting the general behavior of irregular eutectics by making several modifications to the Jackson-Hunt [12] theory, which describes the average undercooling, ΔT, as a function of a spacing parameter, λ,

$$\Delta T = K_1 v\lambda + \frac{K_2}{\lambda} \tag{1}$$

where, for a given alloy, K_1 and K_2 depend on solute diffusivity and interfacial free energy, respectively, and are generally taken as constant. A key component of the theory is the assumption that, for a constant velocity, the overall structure will naturally select the minimum undercooling state and that appropriate adjustment mechanisms are operative to facilitate such selection . From Eq.(1), this *extremum* state is described as

$$\lambda^2 v = \frac{K_2}{K_1}, \tag{2}$$

a condition which has indeed been experimentally demonstrated to be favored in a number of regular eutectic systems [17,18].

It is imperative to note here that λ is well defined only for *regular* periodic assemblages of lamella or rods and that the calculation of average interfacial curvature and composition, leading to the two undercooling terms in Eq.(1), is critically dependent on this regular periodicity. These limitations are evident in the breakdown of the theory with regard to its general applicability to irregular eutectic growth, as evidenced by the varied measurements of selected eutectic operating state. Such reports are listed in Table II, indicating that the factors governing the selection of the eutectic operating point may not be well definable within the framework of the model. We note further that the deficiency is not due to the improper description of the relationship between average eutectic spacing and average undercooling. Rather, the principal problem is that the sole microstructural parameter, λ, is ill-defined for the irregular structure. Thus, while the theory reasonably describes the relationship between average undercooling and some *effective* spacing, the relationship between the *local* morphology and the overall average undercooling remains unclear. This shortcoming is most evident in the prediction of operating range and growth mode transitions, where the local mechanisms of morphological adjustment are critical.

Table II. Reported mean spacing-velocity behavior for Al-Si eutectic solidification.

Authors / Reference	Year	$\lambda - v$ Relationship (λ in μm and v in μm/s)	Gradient (K/mm)	Velocity Range (μm/s)	Comp. (wt% Si)
Toloui, Hellawell [10]	1976	$\lambda^{2.48}v = 10390$	0.7	20 - 400	12.9
		$\lambda^{2.48}v = 4624.8$	1.5	20 - 400	12.9
		$\lambda^{2.3}v = 1887.6$	4.5	20 - 400	12.9
		$\lambda^{2.09}v = 921.6$	8	20 - 1200	12.9
		$\lambda^{2.02}v = 604.7$	15	20 - 400	12.9
Elliott, Glenister [20]	1980	$\lambda^{3.30}v = 35362.8$	0.8	10 - 165	12.7
Atasoy [6]	1984	$\lambda^{2.27}v = 4082.5$	12	10 - 1266	12.7
		$\lambda^{2.53}v = 5259.3$	12	10 - 950	13.17
		$\lambda^{2.42}v = 2496$	12	10 - 1266	13.43
Hogan, Song [21]	1987	$\lambda^{2.22}v = 1038$	11	10 - 200	12.6
Liu, Zhou, Shang [22]	1990	$\lambda^{3.31}v = 37069.5$	0.8	10 - 165	12.62
Magnin, Mason, Trivedi [19]	1991	$\lambda^{2.01}v = 1185.8$	8	2 - 500	12.6
Kahn, Ourdjini, Elliott [23]	1992	$\lambda^{2.51}v = 5687.9$	3.2	21.6 - 320	–
		$\lambda^{2.24}v = 2237.5$	7.6	28 - 505	–
		$\lambda^{2.61}v = 1950.4$	12.2	28 - 505	–
Wolczynski, Billia, Rabczak [24]	1996	$\lambda^{2.00}v = 359.8$	8	2.6 - 69.4	12.5
Guzik, Kopycinski [25]	1996	$\lambda^{2.87}v = 34482.6$	10.5	2.8 - 111	12.6
Cuprys, Major, Wolczynski [9]	2000	$\lambda^{2.00}v = 605.6$	4	300 - 650	–
		$\lambda^{2.38}v = 795.2$	10	300 - 650	–
Current Study	2003	$\lambda^{2.03}v = 3162.3$ (n_L-based)	7.5	9.5 - 1200	13.0
		$\lambda^{1.92}v = 1341.7$ (n_A-based)	7.5	9.5 - 1200	13.0

Modifications to the JH theory have taken some account of the nonisothermal nature of the interface [13,14,15] and the range of eutectic spacings that generally develop. For example, Magnin and Kurz [15] defined a nonisothermal correction to the average undercooling which is simply added to the undercooling described in Eq.(1). The range of spacings exhibited by the

irregular eutectic has been treated by employing the parameters ϕ and η, which describe the average spacing and the range of spacings, respectively defined as

$$\phi = \frac{\bar{\lambda}}{\lambda_{ext}} \qquad \text{and} \qquad \eta = \frac{\lambda_{max} - \lambda_{min}}{\bar{\lambda}}. \tag{3}$$

Here, $\bar{\lambda}$ is the average spacing, λ_{ext} is the spacing at the extremum, and λ_{max} and λ_{min} are the upper and lower limits to the spacing range, respectively. By adding a nonisothermal correction term to the undercooling in Eq.(1) and establishing criteria for extinction at the minimum spacing and branching at the maximum spacing, Magnin and Kurz [15] theoretically predicted the average operating state as

$$\phi \approx \frac{1}{2} + \left[\left(\frac{f_\beta \Pi_\beta}{P} - 1 \right) \left(f_\alpha + f_\beta \frac{m_\alpha \Gamma_\alpha \sin\theta_\alpha}{m_\beta \Gamma_\beta \sin\theta_\beta} \right) \right]^{\frac{1}{2}} \tag{4}$$

which evaluates to $\phi \approx 4.4$ for the Al-Si eutectic, using the parameters listed in Table III. Magnin et al. [19] have measured both parameters experimentally, finding $\phi = 3.2$ and $\eta = 0.9$ for eutectic growth in aluminum-silicon.

While extensions of the JH treatment have been reasonably successful in predicting observed behavior within certain regimes of growth velocity, the use of a linear spacing parameter and the implied unrealistic 2D description of the interface presents some serious limitations, particularly with respect to the mechanisms of branching and spacing adjustment in irregular eutectics. These issues are critical to establishing the optimization principles for selection of the eutectic operating range and also for describing morphological variations that occur during the quench modification transition. In the work presented here, Al-Si eutectic growth is investigated using directional solidification to (i) examine the mechanisms of spacing adjustment, (ii) characterize the high-rate flake to fiber transition in terms of the three-dimensional morphology, and (iii) identify the velocity range over which these mechanisms operate.

Table III. Physical parameters for the Al-Si eutectic system.

Parameter	Value	Units	Definition
C_{eut}	0.126	---	Eutectic Composition
T_{eut}	850.3	K	Eutectic Temperature
C_α	0.0164	---	Composition (α Phase)
C_β	0.998	---	Composition (β Phase)
m_α	-750	K	Liquidus Slope (α Phase)
m_β	1750	K	Liquidus Slope (β Phase)
ρ_α	2.50E+06	g/m^3	Density (α Phase)
ρ_β	2.15E+06	g/m^3	Density (β Phase)
Γ_α	1.96E-07	mK	Gibbs-Thompson Coefficient (α Phase)
Γ_β	1.70E-07	mK	Gibbs-Thompson Coefficient (β Phase)
θ_α	30	deg.	Three Phase Junction Contact Angle (α Phase)
θ_β	65	deg.	Three Phase Junction Contact Angle (β Phase)
D	4.30E-09	m^2/s	Diffusivity

Solidification Experiments

Alloy test specimens of an Al-13wt%Si alloy were fabricated by vacuum-arc-melting the pure constituents (<10 ppm impurities) on a water-cooled copper hearth, casting into 8 mm billets, swaging to 5 mm diameter rods, and cutting to lengths of 300 mm. Each test specimen was placed into a cylindrical alumina ampoule with an inner diameter of 5.5 mm and directionally solidified in a Bridgman-type furnace. Growth velocities from 10 to 1200 μm/s were employed within a thermal gradient of 7.5 K/mm. For each specimen, the interface was propagated over a total growth distance of approximately 50 mm, followed by quenching into a water-cooled bath of a Ga-In-Sn alloy, yielding a nominal cooling rate of 100 K/s at the growth front.

Analysis of Eutectic Microstructures

The characteristic eutectic structures observed over the range of velocities employed here are shown in Fig.1(a-h). For this series of micrographs, the aluminum-rich solid solution phase has been partially removed by chemical etching to reveal the detailed silicon morphology. These structures suggest that the flake to fiber transition occurs primarily over the velocity range from 100 to 1000 μm/s. However, the very early signs of the transition are evident at velocities as low as 50 μm/s.

Eutectic spacing parameters were measured on transverse sections taken from each specimen at a location within 10 mm of the quenched interface. The quantities n_A and n_L were directly measured, defined as the number of silicon particles per unit area, and the number of Al/Si boundary intersections per unit length, respectively. Based on these measured quantities, we define two distinct spacing parameters, one better suited for the flake morphology and one better suited for the fiber morphology. To accommodate the flake morphology, we define an average flake spacing as

$$\bar{\lambda}_F = \frac{2}{\bar{n}_L}, \qquad (5)$$

where, for each velocity, $\bar{n}_L$ was computed as an average over at least 40 measurements of n_L, each employing a total line length of approximately $75\bar{\lambda}_F$. To best treat the fiber (rod) morphology, assuming that the overall 2D arrangement of rods is roughly hexagonal, the average eutectic rod spacing is defined here as

$$\bar{\lambda}_R = \sqrt{\frac{1}{\bar{n}_A}}\cos\left(\frac{\pi}{6}\right), \qquad (6)$$

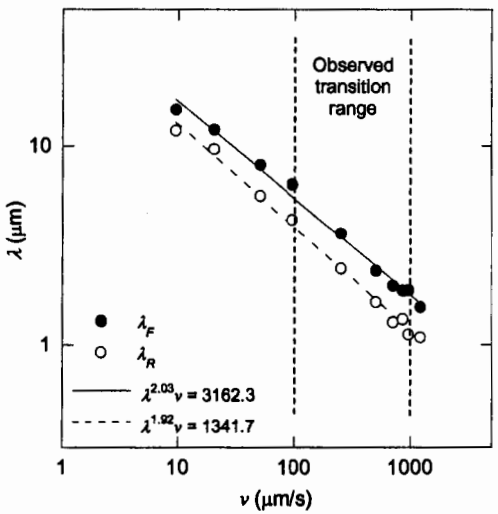

Figure 2. Measurements of eutectic spacing plotted as a function of velocity (measured using both n_A and n_L methods).

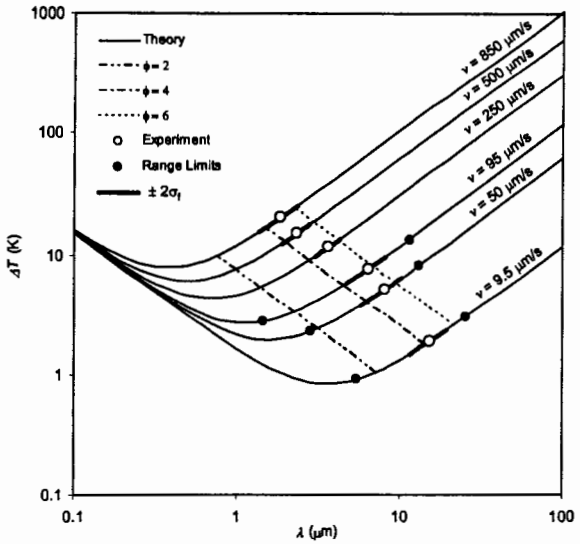

Figure 3. Eutectic spacing measurements plotted on the computed $\bar{\lambda}$-ΔT curves. Open circles show mean spacing measurements. Closed circles show the range of spacings observed. Darkened portions of the curves indicate the range of spacings within 2σ of the mean. The dashed lines indicate several values of the selection parameter, ϕ.

where, for each velocity, $\bar{n}_A$ was computed as an average over 15 measurements of n_A, each employing a total area of approximately $315\bar{\lambda}_R^2$. The experimentally determined values of λ_F and λ_R are plotted as a function of velocity in Fig.2. The velocity regime over which the transition was observed is also indicated. In addition, the experimentally determined constants, indicating the average operating point, are shown in this figure (and listed in Table II). Each parameter was measured over the entire velocity range, but neither reveals any feature that might be indicative of the flake to fiber transition.

Further Analysis and Discussion

The observed eutectic behavior is summarized in the λ-ΔT-v projection plotted in Fig.3. The theoretical λ-v curves were calculated using Eq.(1) with the appropriate nonisothermal correction [15], employing the parameters listed in Table III. The curves for velocities of 250 μm/s and below were computed assuming an irregular lamellar structure. For higher velocities, a regular rod structure was assumed. The open circles in Fig.3 represent the global mean in eutectic spacing, $\langle\bar{\lambda}\rangle$, for each velocity. The bold region of each λ-v curve represents the range of observed local average eutectic spacings, bounded by $\langle\bar{\lambda}\rangle \pm 2\sigma$, where σ is the standard deviation of the measured values of $\bar{\lambda}$, each of which is an average itself, as discussed previously. This measurement of spacing variation should not be mistaken for the operating range of the irregular eutectic structure, which varies between the minimum and maximum values, λ_{min} and λ_{max}, presumably governed by a capillarity limit and a branching limit, respectively. Measured values of λ_{min} are also plotted in Fig.3 for velocities exhibiting a flake morphology. The plotted values of λ_{max} were computed as $(2\bar{\lambda} - \lambda_{min})$, and the operating range parameter was determined from Eq.(3) as $\eta \approx 1.22$.

Regarding the selection of the average eutectic operating state, several dashed lines are plotted in Fig.3 corresponding to several values of the selection parameter, ϕ. Our results suggest a

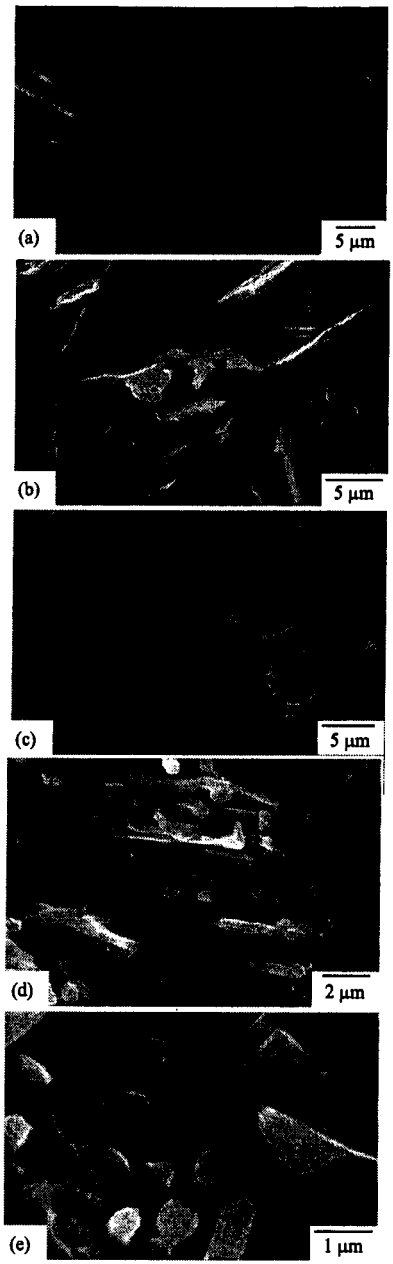

selection parameter of $\phi \approx 5$, a value that is somewhat higher than that reported by Magnin, et al. [19]. In addition, Fig.3 suggests that ϕ may exhibit a velocity dependence, where Magnin et al. reported that ϕ is independent of growth velocity [19]. We point out here that they report values of ϕ for velocities not exceeding 500 μm/s and also note that their data show increased variation above approximately 100 μm/s. Their results, therefore, are not necessarily inconsistent with our findings. Moreover, Magnin et al. [19] conclude that the velocity independence of ϕ indicates that the mechanisms of selection are not changing over that velocity regime. We quite agree, and add that the velocity dependence we observe at higher rates suggests a change in the mechanisms of spacing adjustment and operating point selection over this velocity regime.

The gradual nature of the flake to fiber transition is shown in Fig.4. Qualitatively, it appears that there are two somewhat overlapping but distinct regimes of the transition. In the low-velocity stages (roughly 100-500 μm/s), there is the in-plane break-up of the broad plates into skeletal plates, lamellar rods, and random planar rods, as shown in Fig.4(a,b). In each of these cases, the continuous plate structure is not completely stable and rodlike structures evolve within the envelope of the plates. This is a reasonable progression since the plate itself is aligned along a kinetically favorable direction. These rodlike structures, therefore, involve the transition to more isotropic growth within the plane of the plate, as more in-plane directions become active at higher undercoolings. Out of plane directions remain unfavorable. During these stages of the transition, the eutectic behaves much like an irregular lamellar eutectic (i.e. the flake morphology). Because in-plane rod formation is relatively close range, local rod spacing is not particularly important and the overall growth remains limited by the diffusion distances defined by the remnant plate spacings. The higer-velocity stages of the transition (roughly 500-1000 μm/s) involve a shift to rod-dominated growth as out-of-plane crystallographic directions become favorable. Accordingly, the remnant plate structure gradually

Figure 4. Some details of the high-rate growth-mode transition observed in Al-Si. Growth velocities here are (a) 50, (b) 250, (c) 500, (d,e) 950 μm/s. Early stages of the transition involve rodlike growth within the overall plate structure. Out-of-plane growth and a shift to true rod-dominance occurs at higher velocities as shown in (d-e).

disappears and the relevant diffusion fields become defined by the local rod spacings. The out-of-plane growth that occurs during these later stages of the transition is shown in Fig.4(c,d). When the structure is fully governed by the local rod spacing and optimization involves spacing adjustment in all directions (i.e. at approximately 1000 μm/s), the transition is complete.

We have stated that the principal deficiency with the conventional theory is that the definition of the *eutectic spacing* implies a two dimensional geometry. Indeed, it is clear from the microstructures in Fig.1 and Fig.4, that the irregular eutectic morphologies observed in the Al-Si system cannot be well represented in two dimensions. Thus, any model which relies on a simple linear spacing as the sole microstructural parameter will be inherently limited, particularly with respect to describing any adjustment mechanisms or growth-mode transitions. Accordingly, we seek the definition of a characteristic length scale that is derived from the three-dimensional character of the eutectic structure. Any useful characteristic length would define the scale of spatial variation and, therefore, a representative volume element. Furthermore, any complete description of such a representative volume element would include all stereological parameters that are necessary to describe both the local behavior of the interface as well as the average global behavior. This would necessarily include parameters that quantify the particle shape, size, morphological texture, crystallographic texture, and the spatial variation of these quantities. Such a descriptor is beyond the scope of the current work. However, to illustrate the importance and potential benefit in defining a more comprehensive spacing parameter, we examine here a very simple characteristic length scale, defined as the minimum diameter of a cylinder aligned along the growth direction, within which the relative phase fractions are representative of the overall values. This diameter, d_f, was estimated here experimentally for selected growth velocities in the following way. For a given growth velocity, the area fraction of the silicon phase was measured using circular sampling areas that vary in diameter. Many measurements were made for any given diameter. The silicon phase fraction mean, $\bar{f}_{Si}$, and standard deviation, σ_f, were computed for each diameter. For each velocity, the normalized standard deviation was plotted as a function of sampling area diameter and fitted as an exponentially decaying function. Using the resulting relationships, we estimated the characteristic length, d_f, defined as the diameter at which the standard deviation falls below 10% of the mean, i.e. where

$$\frac{\sigma_f(d_f)}{\bar{f}_{Si}} = 0.1. \qquad (7)$$

The values of d_f determined in this manner are plotted in Fig.5 as a function of velocity. Unlike the conventional spacing parameters, two clear regimes are indicated by the velocity dependence of this characteristic length scale, with a transition indicated at approximately 500 μm/s. Although d_f is overly simple, this result, perhaps, indicates a shift from plate-spacing dominance to rod-spacing dominance, as discussed previously.

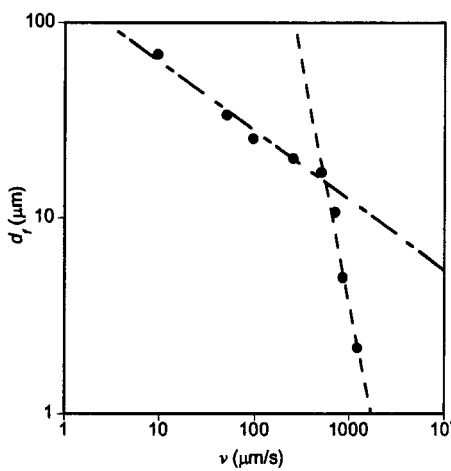

Figure 5. Characteristic length, d_f, as a function of velocity, revealing a transition at approximately 500 μm/s.

Conclusions

For a temperature gradient of 7.5 K/mm, the flake to fiber transition occurs over a wide temperature range. The transition begins gradually at velocities between 50 and 100 μm/s, and continues until the rod behavior becomes fully dominant at approximately 1000 μm/s. Within the transition, a bimodal behavior is apparent, where the rods grow within remnant plate envelopes at lower velocities. Out-of-plane growth becomes more prevalent at higher velocities until the remnant flake structure disappears completely. Traditional spacing measurements, using both lineal and areal methods, failed to identify any growth mode transition. The transition was clearly indicated, however, by the characteristic decay length for the variation in phase fraction as a function of the diameter of the sampling volume. This suggests that a more comprehensive microstructural descriptor is required for prediction of growth mode transitions and operating range selection in irregular eutectics.

Acknowledgements

The research summarized here was made possible by funding from the National Science Foundation, Division of Materials Research (Grant #DMR0237566).

References

1. Shamsuzzoha, M. and Hogan, L. M., *J. Cryst. Growth* **72** (1985) 735.
2. Major, J. F. and Rutter, J. W., *Mat. Sci. Tech.* **5** (1989) 645.
3. Pacz, A., *U.S. Patent No. 1,387,900* (1921).
4. Steen, H. A. H. and Hellawell, A., *Acta metall.* **20** (1972) 363.
5. Atasoy, O. A., *Aluminum* **60** (1984) 239.
6. Lu, Shu-Zu. and Hellawell, A., *J. Cryst. Growth* **73** (1985) 316.
7. Day, M. G. and Hellawell, A., *Proc. Roy. Soc.* **A305** (1968).
8. Cuprys, R., Major, B., and Wolczynski, W., **329-330** (2000) 161.
9. Toloui, B. and Hellawell, A., *Acta metall.* **24** (1976) 565.
10. Khan, S and Elliott, R., *J. Mat. Sci.* **31** (1996) 3731.
11. Jenkinson, D. C. and Hogan, L. M., *J. Cryst. Growth* **28** (1975) 171.
12. Jackson, K. A. and Hunt, J. D., *Trans. AIME* **236** (1966) 1129.
13. Sato, T. and Sayama, Y., *J. Cryst. Growth* **22** (1974) 259.
14. Fisher, D. J. and Kurz, W., *Acta metall.* **28** (1980) 777.
15. Magnin, P. and Kurz, W., *Acta metall.* **35** (1987) 1119.
16. Magnin, P. and Trivedi, R., *Acta metall. mater.* **39** (1991) 453.
17. Jordan, R. M. and Hunt, J. D., *Met. Trans.* **2** (1971) 3401.
18. Clark, J. N. and Elliott, R., *Met. Trans.* **7A** (1976) 1197.
19. Magnin, P., Mason, J. T., and Trivedi, R., *Acta metall. mater.* **39** (1991) 469.
20. Elliott, R. and Glenister, S. M. D., *Acta metall.* **28** (1980) 1489.
21. Hogan, L. M. and Song, H., **18A** (1987) 707.
22. Liu, J., Zhou, Y., and Shang, B., *Acta metall. mater.* **38** (1990) 1631.
23. Khan, S., Ourdjini, A., and Elliott, R., *Mat. Sci. Tech.* **8** (1992) 516.
24. Wolczynski, W., Billia, B., and Rabczak, K., *Mat. Sci. For.* **215-216** (1996) 323.
25. Guzik, E. and Kopycinski, D., **41** (1996) 203.